Rapid urbanisation and climate change key drivers of dramatic flood impacts in Nepal

Authors

1. Mariam Zachariah, *Centre for Environmental Policy, Imperial College London, UK*
2. Roshan Jha, *Centre for Climate Studies, Indian Institute of Technology Bombay, India*
3. Arpita Mondal, *Civil Engineering Department, Indian Institute of Technology Bombay, India; Centre for Climate Studies, Indian Institute of Technology Bombay, India*
4. Surendra Rauniyar, *Australian Bureau of Meteorology, Melbourne, Australia*
5. Maja Vahlberg, *Red Cross Red Crescent Climate Centre, The Hague, the Netherlands; Swedish Red Cross, Stockholm, Sweden (based in Ubmeje/Umeå, Sweden)*
6. Bibek Kayastha, *Nepal Red Cross Society, Kathmandu, Nepal*
7. Emmanuel Raju, *Department of Public Health, Global Health Section & Copenhagen Centre for Disaster Research, University of Copenhagen, Denmark*
8. Nick Baumgart, *Department of Public Health, Global Health Section & Copenhagen Centre for Disaster Research, University of Copenhagen, Denmark*
9. Fahad Saeed, *Climate Analytics, Berlin, Germany*
10. Friederike Otto, *Centre for Environmental Policy, Imperial College London, UK*

Review authors

1. Sjoukje Philip, *Royal Netherlands Meteorological Institute (KNMI), De Bilt, The Netherlands*
2. Sarah Kew, *Royal Netherlands Meteorological Institute (KNMI), De Bilt, The Netherlands*
3. Neeraj Sah, *Centre for Ecology and Hydrology, Wallingford, UK*
4. Roop Singh, *Red Cross Red Crescent Climate Centre, The Hague, the Netherlands (based in New Jersey, USA)*
5. Manjeet Dhakal, *Climate Analytics, Kathmandu, Nepal*
6. Julie Arrighi, *Red Cross Red Crescent Climate Centre, The Hague, The Netherlands; Global Disaster Preparedness Centre, American Red Cross, Washington D.C., USA; University of Twente, Enschede, The Netherlands (based in New York, USA)*
7. Madhab Uprety, *Red Cross Red Crescent Climate Centre, The Hague, the Netherlands (based in Kathmandu, Nepal)*
8. Poudel Amar Mani, *Nepal Red Cross Society, Kathmandu, Nepal*
9. Pramod Adhikari, *Nepal Red Cross Society, Kathmandu, Nepal*
10. Arya Regmi, *Nepal Red Cross Society, Kathmandu, Nepal*

Main findings

- The Metropolitan areas of Kathmandu and Lalitpur are highly exposed to flooding due to their geographic location along a valley with few natural drainage points. Rapid urbanisation (386% increase in built up areas between 1990-2020) and deforestation (28% reduction in forest cover from 1989-2019) in the Kathmandu Valley has disrupted natural water processes, increasing surface runoff and overwhelming drainage systems, while building on flood plains and near rivers has increased the exposure of people and assets to floods.
- Nepal has seen many heavy rainfall events followed by severe flooding in the past. Analysing different observation-based datasets, the relative magnitude of the observed event compared to previous years varies between datasets, making it difficult to estimate how rare the event is in today's climate. According to the Department of Hydrology and Meteorology (DHM), Government of Nepal, the rainfall recorded in several stations during the event was the highest in 54 years of measurements (DHM, 08 October 2024); therefore we use a rounded estimate of 1-in-50 years to define the event for the rest of the analysis.
- To assess if human-induced climate change influenced the heavy rainfall, we first determine if there is a trend in the observations. Our best estimate is that heavy 3-day rainfall events have become about 18% more intense and just over twice more likely, but there are substantial differences between the datasets, which limit our confidence in the accuracy of these figures. The trends are stronger in the satellite era, from 1980 onwards.
- To quantify the role of human-induced climate change we analyse climate models with high resolution that are in principle able to simulate the influence of the mountains on rainfall in the study region. Overall, the available climate models indicate a 10% increase in intensity compared to a 1.3C cooler climate, and an increase in likelihood of about 70%. Under a future warming scenario where the global temperature is 2°C higher than pre-industrial levels, climate models predict even heavier 3-day rainfall events, with a further expected increase of about 3% in rainfall intensity. As only the subset of models showing the smallest change in rainfall with global warming have future simulations available, this is a conservative estimate.
- Given the small mountainous region with complex rainfall-climate dynamics, there is a high level of uncertainty in the results. However, the increase in heavy 3-day rainfall events is in line with a large and growing body of scientific evidence on large-scale extreme rainfall in a warming world, including in Nepal, and the physical understanding that a warmer atmosphere can hold more moisture, leading to heavier downpours.
- The floods were well forecasted by the Department of Hydrology and Meteorology (DHM), but warning messages did not focus on the impacts to the Kathmandu Valley specifically, and it's unclear to what extent the warnings led to early action. The Kathmandu Valley is also not the focus of flood risk management efforts in Nepal, as other regions (notably Terai) generally have been classified as high risk and have historically seen highly impactful floods. This presents an opportunity to further scale anticipatory action systems that have been shown to be cost effective in other parts of Nepal to cover highly exposed urban centres like the Kathmandu Valley.
- The 2015 Gorkha earthquake destabilised hillsides and weakened drainage infrastructure, while the COVID-19 pandemic affected the incomes of low and middle class individuals representing long-term compounding factors that increased vulnerability to floods and landslides. Deforestation and rapid urbanisation expansion, especially into river floodplains, increased the number of people in the path of the flood waters. Comprehensive spatial planning, combined with disaster risk reduction and adaptation, effective policy enforcement,

and increased public awareness, are crucial to mitigate flood risks across central and eastern Nepal, including the Kathmandu Valley.

1 Introduction

From 26th to 28th of September, 2024 extremely heavy rainfall hit large parts of Nepal, particularly the capital and surrounding regions. This led to devastating flash floods in the Koshi basin and riverine flooding from the Bagmati, Sapakoshi, and Nakkhu rivers, causing widespread devastation across several districts in Nepal, particularly in Kathmandu valley. The city saw unprecedented rainfall (CNN, 2024), with 11 stations inside the valley monitored by the Department of Hydrology and Meteorology (DHM) under Government of Nepal breaking their previous records of extreme 24-hour rainfall (DHM 2024). Some areas received up to 323.5 mm (12.7 inches) on 28 September (DHM, 8 October 2024), which pushed the Bagmati River to 2.2 metres above the danger mark (France 24, 2024). Landslides have further compounded the disaster, resulting in widespread destruction. In total, 244 people were killed (Asia News Network, 2024)

The disaster has also severely impacted transportation, with 19 major roads, including highways, either damaged or destroyed (onlinekhabar, 2024). Kathmandu was cut off for the weekend as landslides blocked all three highways out of the city. Although the Prithvi Highway has been temporarily reopened, debris removal continues. Landslides have also obstructed roads across western and southern Nepal, including the Kaligandaki corridor, a crucial route for the districts of Baglung, Parbat, and Syangja. Additionally, the Araniko Highway northeast of Kathmandu, a critical corridor for supplies from China, remains blocked.

Flooding is particularly severe in the low-lying areas of Makawanpur, Kathmandu, Sarlahi, and Mahottari. This has been exacerbated by the release of water through both gates of the Kulekhani Dam, an action taken for only the second time in 25 years. Road blockages between India and Nepal have caused a sharp rise in market prices, adding to the challenges faced by the affected communities. The heavy rainfall and flooding event also resulted in damages, particularly in the state of Bihar in India where some of these rivers flow downstream. As many as 16 districts in Bihar in India are affected by floods from the swelling rivers Kosi, Gandak and Bagmati (The Hindu, 2024).

The event was caused by a synoptic-scale low-pressure area over northern India and a secondary cyclonic vortex over western India, inducing a deep cyclonic circulation and moisture convergence in the region. The interaction between two systems formed the mid-tropospheric vortex extending from Western India to Central Nepal (see Figure. 1.1), which are known to enhance the organisation and longevity of convective systems (Nikumbh et al., 2020). The mid-tropospheric vortex drove strong southwesterly winds from the Arabian Sea and Bay of Bengal towards the Himalayas. This synoptic system combined with the local topography set the stage for extreme rainfall over Central Nepal. This type of low-pressure system has been found to be responsible for large-scale extreme rainfall, increasing significantly over central India since 1980 (Nikumbh et al., 2019).

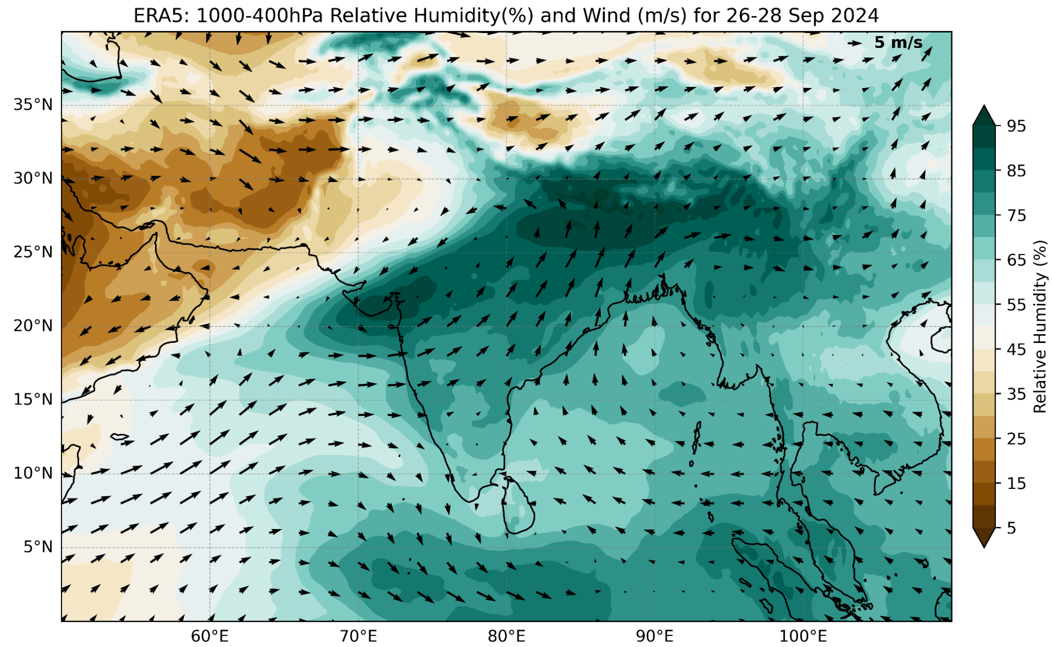

Figure 1.1: *Average Relative Humidity and wind averaged over 1000-400hPa during the heavy rainfall episode over Nepal based on ERA5.*

1.1 Past events in the region

Nepal is often described as one of the most vulnerable countries to the impacts of climate change (World Bank, 2024). Apart from glacier melt, that increases the risk of landslides, affects freshwater availability and can also cause flooding, the increase in heavy rainfall, especially on the short time scales of up to 3 days, is one of the most concerning impacts that has been observed and is projected to increase further with future warming (Talchabhadel et al., 2018).

The Kathmandu Valley is shaped like a basin, with a bowl-like structure that has limited outflow points, making natural drainage difficult, especially during heavy rainfall (Chaulagain et al. 2023). The valley is drained primarily by the Bagmati River, along with its tributaries such as the Bishnumati, Manohara, Dhobi Khola, and Tukucha rivers. These rivers often overflow during intense rains, leading to frequent flooding. The Bagmati River, as the valley's main drainage system, exits through a narrow gorge at Chobhar in the south. However, this single outflow point is insufficient to handle the high volumes of water during heavy monsoon rains, resulting in river overflows and widespread flooding.

The valley has a dense network of rivers and streams that all eventually flow into the Bagmati system. During periods of heavy rainfall, this system can become easily overwhelmed, causing severe flooding. Surrounding the valley are mountain ranges such as Shivapuri, Phulchowki, Nagarjun, and Chandragiri. These hills act as watersheds, collecting and channelling rainfall into the valley's rivers. During the monsoon season, water flows rapidly down these hills, further increasing the volume in the valley's rivers. The steep slopes of these hills exacerbate the runoff, putting even more stress on the valley's already limited drainage capacity.

According to Chaudhary et al. (2024), both rainfall intensity and elevation are the dominant factors driving flood susceptibility in the region. The combination of rapid runoff from the hills and the limited capacity of the valley's river system significantly increases the risk of flooding during heavy rains.

In combination with this geography, climate change, which is projected to increase heavy rainfall and subsequently flood risk in Nepal, poses a very high risk in densely populated areas, including the city of Kathmandu (Shreshta et al., 2023). In addition to climate change and the geography of the country, rapid urbanisation in Kathmandu has been identified as an additional driver of flood risk in the Metropolitan area (Sourav et al., 2021).

1.2 Event Definition

Figure 1.2 shows the accumulated rainfall during this period in three gridded datasets- MSWEP, ERA5 and CPC. According to National Disaster Risk Reduction and Management Authority (NDRRMA) site reports (NDRRMA, 29 September 2024; 1 October 2024), the impacts of the heavy rainfall during the three days (26-28 September 2024) were spread across 22 districts in the central and southern part of the country where most of this rain fell. This region is highlighted in red and selected as the study domain for this study. It is also worth noting that the selected region is fairly homogeneous in terms of terrain and climate and does not contain the western part of Nepal where there is a negative trend in seasonal rainfall associated with high pressure systems that causes increasing dry and cold air influx from the Tibetan Plateau, as opposed to increasing trends over the rest of the country associated with the warm and moist air coming in from the Bay of Bengal (Pokharel et al., 2020). The rainfall cycle in Nepal runs from Jan-Dec, with the rainy season during June-September. Therefore the annual maximum 3-day accumulated rainfall (annRx3day) area-averaged over the study region is chosen as the event definition for the attribution study.

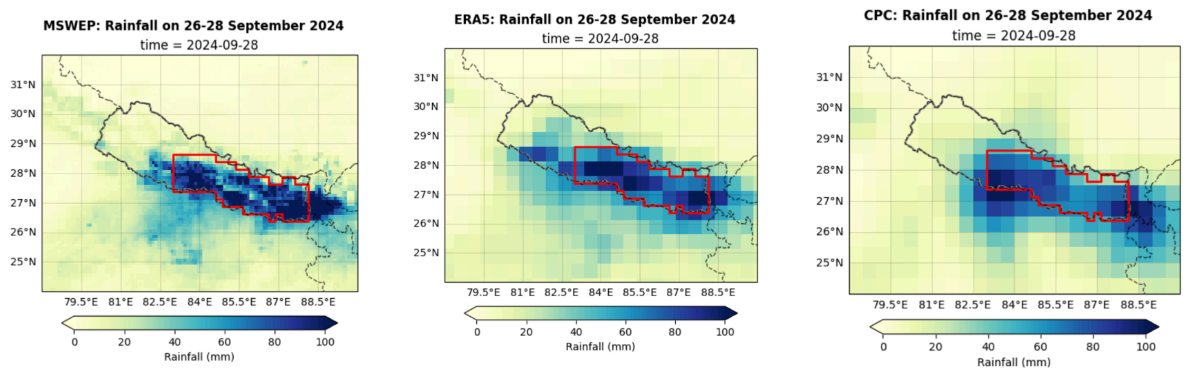

Figure 1.2: *Three days of rainfall during 26-28 September, 2024 in (a) MSWEP (b) ERA5 and (c) CPC gridded datasets. The red highlight indicates the study region.*

In this report, we study the influence of anthropogenic climate change by comparing the likelihood and intensity of a similar annRx3day at present with that in a 1.3 °C cooler climate. We also extend this analysis into the future by assessing the influence of a further 0.7 °C of global warming from present.

2 Data and methods

2.1 Observational data

Four gridded datasets were considered in this study for analysing rainfall extremes in the region:

1. *CPC gridded rainfall* from Climate Prediction Centre (CPC), a product from NOAA PSL, Boulder, Colorado, USA and known as the CPC Global Unified Daily Gridded data. This is available from NOAA at 0.5° spatial resolution covering the period 1979-present.
2. MSWEP gridded rainfall dataset, or the Multi-Source Weighted-Ensemble Precipitation (MSWEP) dataset (updated from Beck et al., 2019) is a product that combines gauge-, satellite-, and reanalysis-based data for reliable precipitation estimates, at daily intervals from 1979 to near real-time, and at 0.1° spatial resolution globally.
3. *ERA5 Reanalysis v5 gridded rainfall* from the European Centre for Medium-Range Weather Forecasts (ECMWF) which starts in the year 1940 (Hersbach et al., 2020), and available at 0.25° spatial resolution. It should be noted that the variables from ERA5 are not directly assimilated, but these are generated by atmospheric components of the Integrated Forecast System (IFS) modelling system. Daily rainfall data from this product starting from the year 1950, available at 0.5° × 0.5° from the Climate Explorer was utilised for this study. At the time, the re-analysis was available until the end of August 2024. This was extended with the ECMWF analysis (1-30 September) to cover the days including the day of the event.
4. CHIRPS gridded rainfall dataset developed by the UC Santa Barbara Climate Hazards Group or the "Climate Hazards Group InfraRed Precipitation with Station data" (CHIRPS; Funk et al. 2015). Daily data are available at 0.05° resolution, from 1981-31August 2024. The product incorporates satellite imagery with in-situ station data. Whilst this product does not yet include the dates of the event, it is still used in the trend assessment of similar past events.

As a measure of anthropogenic climate change we use the (low-pass filtered) global mean surface temperature (GMST), where GMST is taken from the National Aeronautics and Space Administration (NASA) Goddard Institute for Space Science (GISS) surface temperature analysis (GISTEMP, Hansen et al., 2010 and Lenssen et al. 2019).

2.2 Model and experiment descriptions

For this study, we use two multi-model ensembles from climate modelling experiments which have high enough resolution to satisfactorily represent the region and using very different framings (Philip et al., 2020): Sea Surface temperature (SST) driven global circulation high resolution models, and regional climate models,.

1. **CORDEX**-WAS-22 model ensemble: Coordinated Regional Climate Downscaling Experiment CORDEX-CORE over the West-Asia domain with 0.22 km resolution (WAS-22) (Teichman et al., 2021). The ensemble consists of 3 regional climate models downscaling 6 GCMs. These simulations are composed of historical simulations up to 2005, and extended to the year 2100 using the RCP8.5 scenario.

2. **HighResMIP** SST-forced model ensemble (Haarsma et al. 2016), the simulations for which span from 1950 to 2050. The SST and sea ice forcings for the period 1950-2014 are obtained

from the 0.25° x 0.25° Hadley Centre Global Sea Ice and Sea Surface Temperature dataset that have undergone area-weighted regridding to match the climate model resolution (see Table B). For the 'future' time period (2015-2050), SST/sea-ice data are derived from RCP8.5 (CMIP5) data, and combined with greenhouse gas forcings from SSP5-8.5 (CMIP6) simulations (see Section 3.3 of Haarsma et al. 2016 for further details).

2.3 Statistical methods

Methods for observational and model analysis and for model evaluation and synthesis are used according to the World Weather Attribution Protocol, described in Philip et al., (2020), with supporting details found in van Oldenborgh et al., (2021), Ciavarella et al., (2021) and here. The key steps, presented in sections 3-6, are: (3) trend estimation from observations; (4) model validation; (5) multi-method multi-model attribution; and (6) synthesis of the attribution statement.

In this report we analyse time series of annual maximum 3-day rainfall total area-averaged over the study region. A nonstationary generalised extreme value (GEV) distribution is used to model annRx3day from daily rainfall area-averaged over the study region. The distribution is assumed to scale exponentially with GMST, with the dispersion (the ratio between the standard deviation and the mean) remaining constant over time, while the variance remains constant, as described below:

$$X \sim GEV(\mu, \sigma, \xi \,|\, \mu_0, \sigma_0, \alpha,, T),$$

where X denotes the variable of interest, rainy-season precipitation; T is the smoothed GMST; μ_0, σ_0 and ξ are the location, scale and shape parameters of the nonstationary distribution; and α is the trend due to GMST. As a result, the location and scale of the distribution have a different value in each year, determined by both the GMST and Niño3.4 states. Maximum likelihood estimation is used to estimate the model parameters, with

$$\mu = \mu_0 exp\left(\frac{\alpha T}{\mu_o}\right) \quad \text{and} \quad \sigma = \sigma_0 exp\left(\frac{\alpha T}{\mu_o}\right).$$

This formulation reflects the Clausius Clapeyron relation, which implies that precipitation scales exponentially with temperature (Trenberth et.al., 2003, O'Gorman and Schneider 2009). The parameters of the statistical model are estimated using maximum likelihood. For each time series, we calculate the return periods, probability ratio (PR; the factor-change in the event's probability) and change in intensity of the event under study for the 2024 GMST and for 1.3 C cooler GMST: this allows us to compare the climate of now and of the preindustrial past (1850-1900, based on the Global Warming Index).

3 Observational analysis: return period and trend

3.1 Analysis of gridded datasets

The left panels in Figure 3.1 shows the response of annual maximum 3-day rainfall area-averaged over the study region to the global mean temperature, based on the MSWEP, ERA5 and CHIRPS datasets. There is an increasing trend in the intensity of Rx3day in MSWEP and ERA5 (when considering 1979-2024) in response to global warming, while the trends border on no change when considering the data from 1950 in ERA5 and decreases in CHIRPS. At the time of doing the analysis, the CHIRPS data is available only until August 2024, and therefore does not cover the event. The right panels in Figure 3.1 shows the return period curves, for the 2024 climate and a 1.3 °C cooler climate. The 2024 event has a return period of 20 years in the MSWEP dataset; in ERA5, the event has a return period of 12 years when considering from 1950, and 6 years when considering from 1979 onwards. In MSWEP, the return period of the 2024 event is 20 years. (See Table 3.1 for uncertainty ranges). However, due to the hilly terrain, the small size of the study region and limited knowledge on the aptness of the selected gridded datasets in capturing rainfall in this region, and the disagreement in trends (left panels; Figure 3.1), it is difficult to trust one of these datasets over the others. According to Department of Hydrology and Meteorology (DHM), the rainfall recorded in several stations during the event was the highest in their 54 years of measurements since records began in 1970 (Red Cross Red Crescent Climate Centre, 29 September 2024); therefore we use a rounded estimate of 1-in-50 years to define the event for the rest of the analysis.

The probability ratio and intensity changes between the 2024 climate and a 1.3degC cooler climate (before humans began warming the planet), for an event such as the 2024 event are shown in Table 3.1. These metrics are highest in the shorter time series from ERA5 (considering 1979 onwards) with a best-estimated PR of 17 and 65% increase in magnitude. The estimates are similar for MSWEP with PR of 14 and magnitude increase of 64%. In ERA5 (considering 1950 onwards), the estimates suggest no change in the likelihood and intensity with best estimated PR of 0.85 and a decrease in intensity change of 3%. We do not know whether the difference with the trend from 1979 onwards is due to data quality or a change in trends due to other factors. Due to the decreasing trend observed in CHIRPS, the best estimated PR of the 1-in-50 year event is 0.13 (~8 times less likely due to climate change) along with a best estimated 27% decrease in the intensity due to climate change till now.
It should be noted that the CPC dataset which was also considered in the study as an independent source of observations was discarded prior to this step- because although the dataset had a good representation of the event, it underestimates the magnitudes of the extremes and shows a steep increase in trend since 2000 as compared to the other gridded datasets. Therefore, and because we do not have good reasons to choose either the 1979-2040 or 1950-2024 period, for the synthesis of the observed trends we use MSWEP, ERA5 for both 1979-2024 and 1950-2024 and CHIRPS. We acknowledge that the results are sensitive to this choice, but also stress that the direction of change is clear.

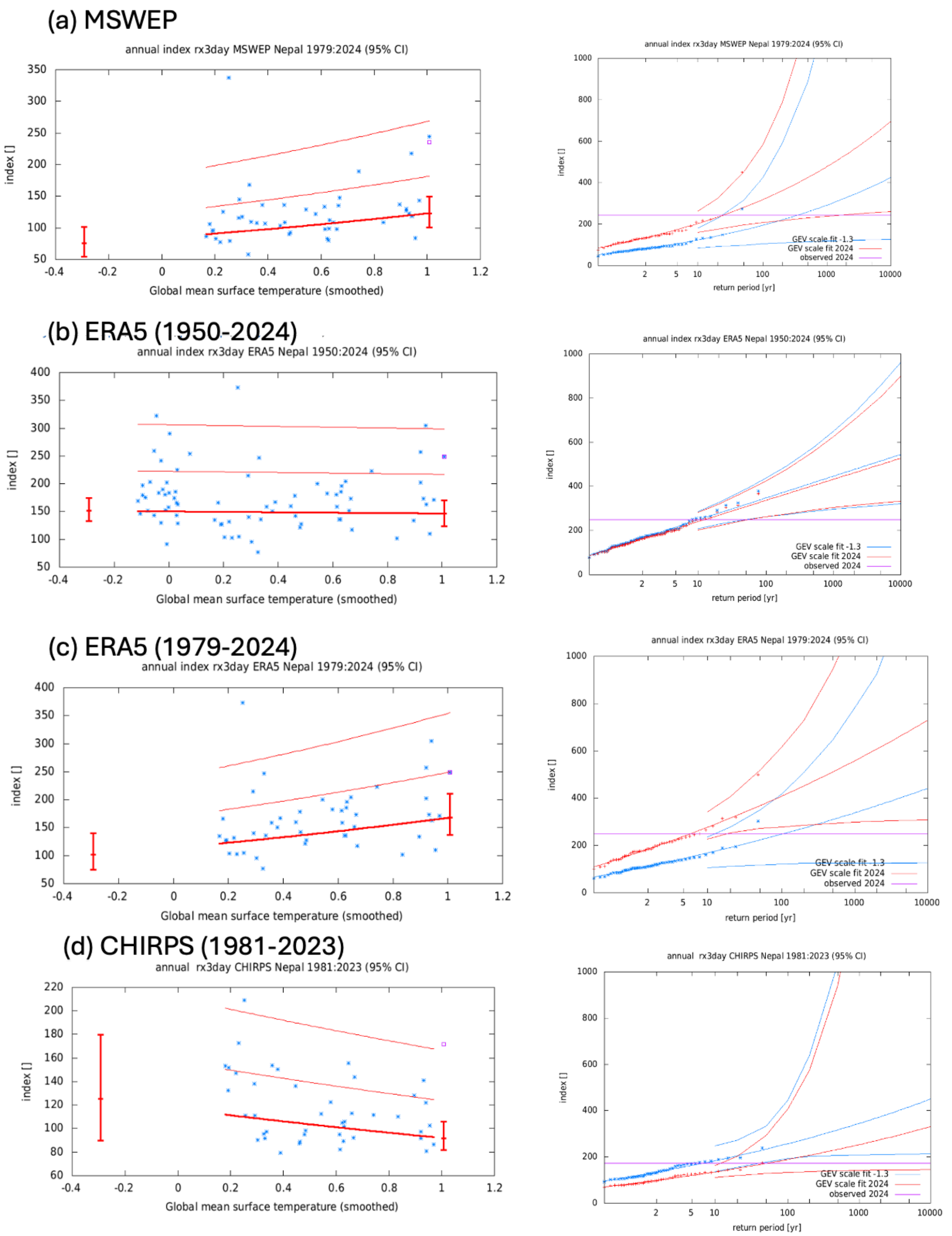

Figure 3.1: *GEV fit with constant dispersion parameters, and location parameter scaling proportional to GMST of the index series, for the study region based on three gridded datasets- (a) MSWEP(b) ERA5 (1950 -2024) © ERA5 (1979 - 2024) and (d) CHIRPS. The 2024 event is included in the fit.* ***Left****: Observed annual (Jan-Dec) max.3-day accumulated rainfall as a function of the smoothed GMST. The thick red line denotes the time-varying location parameter. The vertical red lines show the 95% confidence interval for the location parameter, for the current, 2024 climate and a 1.3ºC cooler climate. The 2024 observation is highlighted with the magenta box.* ***Right****: Return time plots for the climate of 2024 (red) and a climate with GMST 1.3 ºC cooler (blue). The past observations are shown twice: once shifted up to the current climate and once*

shifted down to the climate of the late nineteenth century. The markers show the data and the lines show the fits and uncertainty from the bootstrap. The magenta line shows the magnitude of the 2024 event analysed here.

Table 3.1: *Estimated return periods of annual rx3day over Nepal in the three reanalysis datasets (MSWEP, ERA5 and CHIRPS) with coverage of the event and the estimated magnitude of the 1-in-50 year event in the CHIRPS datasets. Change in probability ratio and magnitude for annual rx3day in the study region due to GMST. Light blue indicates an X increasing trend that crosses no change, while dark blue indicates a statistically significant increasing trend. Light orange indicates a decreasing trend, while dark orange indicates a statistically significant decreasing trend.*

Dataset	Event		GMST (Covariate)	
	Magnitude (mm)	Return period (95% C.I.)	Probability Ratio	Change in magnitude (%)
MSWEP	235.07 mm	20 (7.0 ... 7.1e+3)	14 (1.1 ... 2.6e+4)	64 (3.1 ... 1.7e+2)
ERA5 (from 1950)	248.83 mm	12 (6.0 ... 61)	0.83 (0.15 ... 5.3)	-3.1 (-27 ... 25)
ERA5 (from 1979)	248.83 mm	6.0 (3.0 ... 22)	17 (1.0 ... 8.9e+4)	65 (-0.0070 ... 1.7e+2)
CHIRPS	171.68 mm	50 (50 ... 50)	0.13 (0.000012 ... 1.7e+11)	-27 (-53 ... 14)

4 Model evaluation

In general, CMIP5 and CMIP6 GCMs are known to perform well in terms of capturing the broader spatial and temporal patterns and timing of peaks in daily rainfall for the wider southeast Asian domain (Khadka et al., 2021); however this does not extend to all subregions, thus requiring high-resolution climate models such as those from the HighResMIP and the dynamically downscaled CORDEX modelling experiments. Over the Himalayan region where the study domain is located, orographic interactions are an important driver of precipitation mechanisms needing high-resolution dynamically downscaled models that can simulate these. Assessments of models under the CORDEX-WAS experiment in this region conclude that the models simulate the evolution and trends of seasonal precipitation but with some uncertainty arising from the model physics, they show dry biases in the foothills progressing into wet biases at higher elevations and the ensemble outperforms individual model outcomes (Ghimire et al., 2015; Choudhary and Dimri., 2017). These aspects are also observed in other studies assessing the fidelity of CORDEX models at regional to city-scales for various indicators including extreme precipitation indices such as wet-day frequency and n-day intensity (Shahi, 2022; Neupane et al., 2021). Overall, all models are found to perform well for capturing the observed spatial patterns of extreme precipitation indices (Shahi, 2022). Evaluation of the precipitation trends over the monsoon region shows uncertainty in the trends due to the differences in the simulation of key processes like convection and local feedback mechanisms in the models. While some models capture the broad regional trends (e.g., decreasing precipitation in the western Himalayas vs increasing in eastern Himalayas discussed in Section 1.2), there is less agreement between the models in consistently simulating the spatial variability in trends, once again due to the misrepresentation of local feedbacks in the model physics and other atmospheric constituents such as aerosols.

In the subsections below we show the results of the model evaluation for each location. For each framing or model setup we also use models that only just pass the evaluation tests if we only have five models or less for that framing that perform well. Table 4.1 shows the model evaluation results.
In this section we show the results of the model evaluation for the assessed region. The climate models are evaluated against the observations in their ability to capture:

1. Seasonal cycles: For this, we qualitatively compare the seasonal cycles based on model outputs against observations-based cycles. We discard the models that exhibit ill-defined peaks in their seasonal cycles. We also discard the model if the rainy season onset/termination varies significantly from the observations.

2. Spatial patterns: Models that do not match the observations in terms of the large-scale precipitation patterns are excluded.

3. Parameters of the fitted statistical models. We discard the model if the model and observation parameters ranges do not overlap.

The models are labelled as ‘good’,’reasonable’, or ’bad’ based on their performances in terms of the three criteria discussed above. A model is given an overall rating of ‘good’ if it is rated ‘good’ for all three characteristics (highlighted in green in Table 4.1). If there is at least one ‘reasonable’, then its overall rating will be ‘reasonable’ and ‘bad’ if there is at least one ‘bad’, highlighted in yellow and red, respectively in Table 4.1. Per framing or model setup we also use models that only just pass the validation tests if we only have five models or less for that framing that perform well. The tables show the model validation results.

Table 4.1: *Evaluation results of the climate models considered for attribution analysis of annual rx3day. For each model, the threshold for a 1-in-50-year event is shown, along with the best estimates of the dispersion and shape parameters are shown, along with a 95% confidence intervals. Furthermore evaluation of the seasonal cycle and spatial pattern are shown.*

Model / Observations	**Seasonal cycle**	**Spatial pattern**	**Dispersion**	**Shape parameter**	**Magnitude of 2024 event (mm)**
MSWEP			0.246 (0.165 ... 0.302)	0.14 (-0.25 ... 0.52)	235.07
ERA5 (from 1950)			0.283 (0.227 ... 0.327)	-0.0010 (-0.17 ... 0.15)	248.83
ERA5 (from 1979)			0.270 (0.194 ... 0.317)	0.061 (-0.42 ... 0.38)	248.83
CHIRPS			0.189 (0.127 ... 0.238)	0.082 (-0.40 ... 0.62)	171.68
					Threshold for return period 50 yr
CORDEX-WAS22 ()					
EC-EARTH_rcp85_r12i1p1_CLMcom-ETH-COSMO-crCLIM-v1-1 historical-rcp85 (1)	reasonable	reasonable	0.288 (0.206 ... 0.355)	-0.15 (-0.42 ... 0.088)	279.289
HadGEM2-ES_rcp85_r1i1p1_GERICS-REMO2015 historical-rcp85 (1)	bad	bad	0.358 (0.234 ... 0.426)	0.0071 (-0.33 ... 0.60)	388.055
MIROC5_rcp85_r1i1p1_ICTP-RegCM4-7 historical-rcp85 (1)	reasonable	reasonable	0.304 (0.211 ... 0.365)	-0.19 (-0.68 ... 0.31)	594.357
MPI-ESM-LR_rcp85_r1i1p1_CLMcom-ETH-COSMO-crCLIM-v1-1 historical-rcp85 (1)	reasonable	reasonable	0.247 (0.178 ... 0.309)	0.13 (-0.26 ... 0.58)	269.554
MPI-ESM-LR_rcp85_r1i1p1_GERICS-REMO2015 historical-rcp85 (1)	bad	bad	0.306 (0.215 ... 0.354)	0.084 (-0.59 ... 0.47)	341.103
MPI-ESM-MR_rcp85_r1i1p1_ICTP-RegCM4-7 historical-rcp85 (1)	reasonable	reasonable	0.228 (0.164 ... 0.278)	0.12 (-0.16 ... 0.45)	601.262
NorESM1-M_rcp85_r1i1p1_CLMcom-ETH-COSMO-crCLIM-v1-1 historical-rcp85 (1)	reasonable	good	0.270 (0.167 ... 0.340)	0.31 (-0.0064 ... 0.99)	301.324
NorESM1-M_rcp85_r1i1p1_GERICS-REMO2015 historical-rcp85 (1)	good	bad	0.255 (0.162 ... 0.315)	0.12 (-0.35 ... 0.89)	392.164

NorESM1-M_rcp85_r1i1p1_ICTP-RegCM4-7 historical-rcp85 (1)	reasonable	reasonable	0.196 (0.0991 ... 0.244)	0.097 (-0.30 ... 0.82)	496.784
(1)			(...)	(...)	
HighResMIP (1)			(...)	(...)	
CMCC-CM2-HR4 histSST-present (1)	bad	reasonable	0.222 (0.144 ... 0.272)	0.24 (-0.18 ... 1.0)	572.909
CMCC-CM2-VHR4 histSST-present (1)	reasonable	good	0.337 (0.259 ... 0.394)	0.054 (-0.36 ... 0.35)	457.246
EC-Earth3P-HR histSST-present ()	good	good	0.274 (0.177 ... 0.333)	0.15 (-0.14 ... 0.67)	294.570
EC-Earth3P histSST-present (1)	good	good			192.623
HadGEM3-GC31-HM histSST-present (1)	good	bad	0.231 (0.169 ... 0.276)	0.049 (-0.42 ... 0.53)	274.311
HadGEM3-GC31-LM histSST-present (1)	good	bad	0.151 (0.116 ... 0.176)	-0.087 (-0.41 ... 0.20)	175.728
HadGEM3-GC31-MM histSST-present (1)	good	bad	0.241 (0.172 ... 0.285)	-0.023 (-0.37 ... 0.35)	275.786
MPI-ESM1-2-HR histSST-present (1)	good	bad	0.136 (0.0788 ... 0.177)	0.15 (-0.33 ... 0.65)	204.384
MPI-ESM1-2-XR histSST-present (1)	good	bad	0.225 (0.140 ... 0.268)	0.28 (-0.13 ... 0.76)	224.365

5 Multi-method multi-model attribution

Table 5.1 shows Probability Ratios and change in intensity ΔI for models that passed model evaluation and also includes the values calculated from the fits with observations.

Table 5.1: *Event magnitude, probability ratio and change in intensity for 100-year return period for annualRx3day event area-averaged over the study region for observational datasets and each model that passed the evaluation tests. (a) from pre-industrial climate to the present and (b) from the present to 2℃ above pre-industrial climate.*

	a. Past vs. present		**b. Present vs. future**	
Model / Observations	**Probability ratio PR [-]**	**Change in intensity ΔI [mm]**	**Probability ratio PR [-]**	**Change in intensity ΔI [%]**
MSWEP	14 (1.1 ... 2.6e+4)	64 (3.1 ... 1.7e+2)		
ERA5 (from 1950)	0.83 (0.15 ... 5.3)	-3.1 (-27 ... 25)		
CHIRPS	0.13 (0.000012 ... 1.7e+11)	-27 (-53 ... 14)		
EC-EARTH_rcp85_r12i1p1_CLMcom-ETH-COSMO-crCLIM-v1-1 historical-rcp85 (1)	3.1 (0.38 ... 1.5e+7)	9.4 (-10 ... 39)	0.87 (0.43 ... 1.6)	-1.4 (-7.6 ... 4.6)

MPI-ESM-LR_rcp85_r1i1p1_CLMcom-ETH-COSMO-crCLIM-v1-1 historical-rcp85 (1)	0.95 (0.41 ... 3.7)	-0.97 (-16 ... 18)	1.0 (0.76 ... 1.5)	0.31 (-5.4 ... 5.5)
MPI-ESM-MR_rcp85_r1i1p1_ICTP-RegCM4-7 historical-rcp85 (1)	2.1 (0.81 ... 14)	16 (-4.6 ... 40)	1.2 (0.84 ... 2.3)	3.9 (-3.9 ... 12)
NorESM1-M_rcp85_r1i1p1_CLMcom-ETH-COSMO-crCLIM-v1-1 historical-rcp85 (1)	1.9 (0.57 ... 2.0e+2)	13 (-12 ... 54)	1.4 (1.0 ... 2.3)	5.9 (0.15 ... 12)
NorESM1-M_rcp85_r1i1p1_ICTP-RegCM4-7 historical-rcp85 (1)	1.3 (0.18 ... 14)	4.3 (-24 ... 36)	1.7 (0.89 ... 4.0)	6.9 (-1.9 ... 14)
CMCC-CM2-VHR4 histSST-present (1)	5.6 (0.57 ... 1.4e+3)	26 (-7.9 ... 65)	(...)	(...)
EC-Earth3P-HR histSST-present ()	5.7 (1.5 ... 54)	43 (11 ... 90)	(...)	(...)
EC-Earth3P histSST-present (1)	1.5 (0.49 ... 8.4)	5.4 (-9.9 ... 25)	(...)	(...)

6 Hazard synthesis

For the event definition described above we evaluate the influence of anthropogenic climate change on the 3-day maximum rainfall in the study region by calculating the probability ratio as well as the change in intensity combining the observation-based assessment and climate models detailed above. Models which do not pass the evaluation described in section 4 are excluded from the analysis. Given that only two models were evaluated as “good” we also include the “reasonable” models in the final assessment. The aim is to synthesise results from models that pass the evaluation along with the observations-based products, to give an overarching attribution statement.

Figure 6.1 shows the changes in probability and intensity for the observations (blue) and models (red). Before combining them into a synthesised assessment, first, a representation error is added (in quadrature) to the observations, to account for the difference between observations-based datasets that cannot be explained by natural variability. This is shown in these figures as white boxes around the light blue bars. The dark blue bar shows the average over the observation-based products. The dark red bar shows the model average, consisting of a weighted mean using the (uncorrelated) uncertainties due to natural variability. Details on this approach can be found in Li and Otto (2022).

Observation-based products and models are combined into a single result in two ways. Firstly, we neglect common model uncertainties beyond the intermodel spread that is depicted by the model average, and compute the weighted average of models (dark red bar) and observations (dark blue bar): this is indicated by the magenta bar. As, due to common model uncertainties, model uncertainty can be larger than the intermodel spread, secondly, we also show the more conservative estimate of an unweighted, direct average of observations (dark red bar) and models (dark blue bar) contributing 50% each, indicated by the white box around the magenta bar in the synthesis figures.

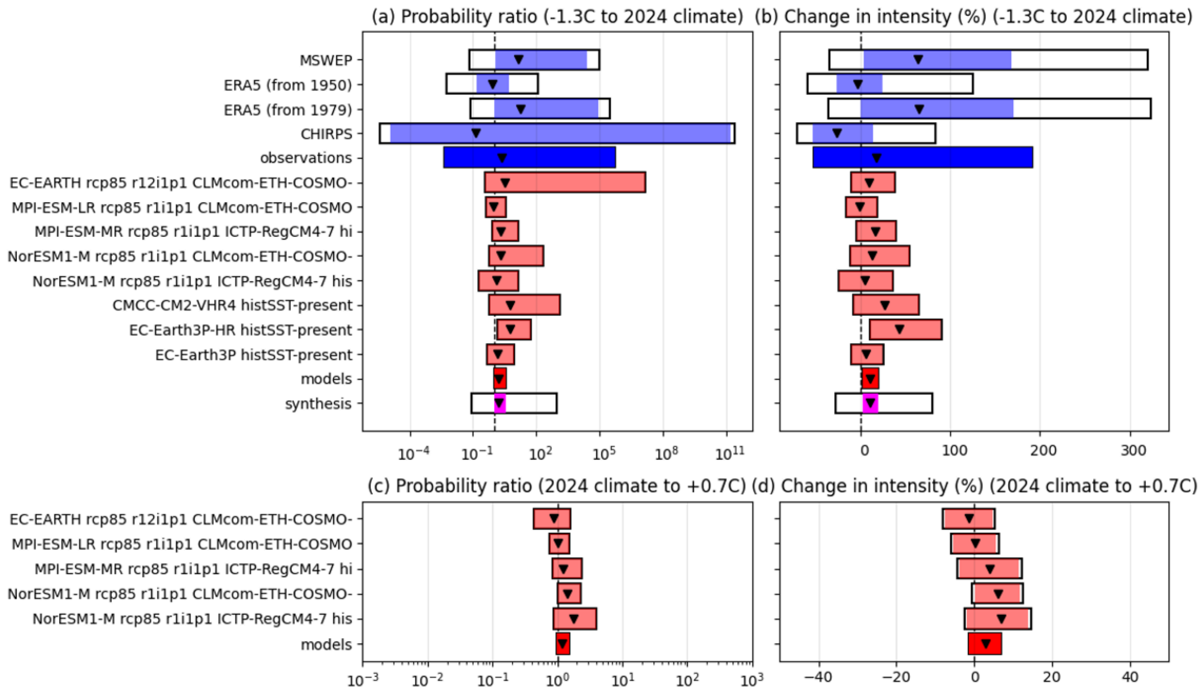

Figure 6.1: *(a) Synthesis of probability ratios and (b) relative intensity changes when comparing the return period and magnitudes of annual rx3day in the study region between the current climate and a 1.3C cooler climate. (c) same as (a) and (d) same as(b) but synthesising changes in annual rx3day between the current climate and a 0.7C warmer climate (that is, a climate that is 2C warmer than preindustrial).*

The combined results for the observations and models as well as the synthesis are also summarised in Table 6.1. Despite the known shortcomings of the models, the model results are all very similar.

However, the observation-based products differ very much and also show a very high uncertainty. Given the topography of the region this is not unexpected. Variability in observed rainfall between different individual locations is very high, thus estimates in any gridded data product will vary depending on the exact number of stations included. The records are generally also short and thus, even if the trend was much stronger than expected from the Clausius-Clapeyron (C-C) relationship, it would not be detectable with statistical significance. Furthermore, the synthesised estimate of the change in intensity and likelihood in observations strongly depends on the exact data sets included. In Table 6.2, we show how the estimate changes from a factor 2.28 (0.456E-02 to 0.536E+06) increase in likelihood and a 17.7% (-52.5% to 191%) increase in intensity to a 5.87 (0.0951 to 0.563E+04) times increase in likelihood and 37.8% (-34.2% to 188%) by excluding the most uncertain, and thus least informative dataset, CHIRPS. Without any station data available we have no means to give one data set more weight or less weight than the others, we thus include all available data sets, but note that the observed changes are only qualitatively useful, rather than quantitatively. We further note that one data set, ERA5, is included twice, from 1950, the start of the available time series, and from 1979, the beginning of the satellite era. This is to highlight that the trends change in sign, depending on the length of the timeseries but also distorts the relative weighting of the available data. The overall synthesised results, which are also near-identical to the synthesised estimates based on the climate models alone (see Table 6.2) show an increase in likelihood of a factor 1.7 (1.1 to 3.8) which we communicate as an increase by about 70% and an increase in intensity of 11% (2.5% to 20.2%), communicated as about 10%, which is in line with the expected increase following the C-C relationship. We have no reason to assume that there are any mechanisms counteracting this relationship in this region, and thus have high confidence in the role of climate change in intensifying rainfall events such as the one under study. The synthesised numbers are also not dependent on the exact treatment of the observation-based results. The assessment does not allow however to assess whether other mechanisms than the thermodynamic warming might be at play, as they would be masked in the high observational uncertainty.

We also report the model based changes in intensity and likelihood in a 0.7C warmer world from today, for the models where future runs are available. It should be noted that these results are based only on the CORDEX models which showed a smaller increase (than expected from the C-C relationship) as compared to the SST-driven HighResMIP for the past-present analysis, and therefore the smaller increase in intensity under future scenario is likely an underestimation. We thus have much lower confidence in these numbers, which are about a 3% increase in intensity, and a 20% increase in likelihood, and assume they are too conservative as there are no known reasons to assume future changes would be lower than expected from thermodynamics.

Table 6.1: *Summary of results for annual Rx3day area-averaged over the study domain, presented in Fig. 6.1: changes due to GMST include past-present changes and present-future changes. Statistically significant increases in probability and intensity are highlighted in dark blue , while non-significant increases are highlighted in light blue.*

Data	GMST	
		Probability ratio (95% CI)	Intensity change (%) (95% CI)
Observations	Past- Present	2.28 (0.456E-02 … 0.536E+06)	17.7 (-52.5 … 191)
Models		1.68 (1.06 … 3.75	10.7 (2.37 … 20.1)
Synthesis		1.69 (1.06 … 3.75	10.8 (2.45 … 20.2)
Models only	Present- Future	1.17 (0.975 … 1.50)	2.83 (-1.39 … 6.95)

Table 6.2: *same as Table 6.1, but showing synthesised estimates of PR and intensity changes but excluding the estimates from CHIRPS in the computation .*

Data	GMST (without CHIRPS)		
		Probability ratio (95% CI)	Intensity change (%) (95% CI)
Observations	Past- Present	5.87 (0.0951 … 0.563E+04	37.8 (-34.2 … 188)
Models		1.68 (1.06 … 3.75)	10.7 (2.37 … 20.1)
Synthesis		1.71 (1.08 3.79)	11 (2.68 … 20.4)
Models only	Present- Future	1.17 (0.975 … 1.50)	2.83 (-1.39 … 6.95)

7 Vulnerability and exposure

In late September 2024, severe rivering and flash flooding and landslides occurred across several regions in Nepal, particularly affecting the central and eastern provinces of Nepal. Impacts are concentrated in districts across Kathmandu Valley (see Figure 7.1), other parts of the hilly region such as Kavre and Sindhuli, and low-lying districts in the lowlands, known as Terai, including Makawanpur, Kathmandu, Sarlahi, Mahottari, and Chitawan (IFRC GO, 2024). The heavy rainfall arrived at the end of the monsoon season when the infiltration capacity of the soil was low, which contributed to the high runoff. These floods caused widespread devastation, including 244 fatalities (Asia News Network, 2024), thousands displaced, and significant damage to homes, infrastructure, and agriculture (ACAPS, 2024). Key sectors such as transportation, health, education, and energy were severely disrupted, with rural and urban communities alike suffering substantial losses.

Preliminary estimates total 17 billion NPR/126,3 billion USD in losses (AA, 2024). The floods and landslides are wreaking havoc in the midst of Nepal's festive season, and just before the country's main holiday, Dashain, inhibiting many families from celebrating together, because of the major disruptions to transportation.

Figure 7.1. *Observed riverine flood extent in the regions of Kathmandu Valley derived from satellite images of 30th September. Source: Department of Hydrology and Meteorology (2024).*

7.1 Flood risk

Flooding is the most frequent and amongst the most impactful natural hazards in Nepal, causing extensive physical and socioeconomic losses (Mesta et al., 2023). The Koshi, Karnali, and Narayani river systems are the largest in the country, and floods from these perennial rivers regularly affect multiple districts, particularly in the southern Terai, identified as the region of Nepal facing the highest flood risk (ADB, 2019). In recent years, impacts from floods from medium and small rivers and rivulets originating in the Chure and Middle Mountains (similar to this event) are becoming more frequent, but tend to be more concentrated to central valleys rather than southern Terai.

While the Kathmandu Valley is not considered one of the flood risk hotspots in Nepal, but instead of "very low risk" to flooding (MoFE, 2022), it does face significant challenges due to its unique urban and geographic conditions. The valley, shaped like a bowl with limited drainage outlets, is prone to waterlogging during heavy rainfall. The Bagmati River, along with its tributaries such as the Bishnumati, Manohara, Hanumante and Tukucha, often overflow during intense rains due to the inadequate drainage capacity. The single outflow point at the narrow Chobhar gorge in the southwest (see Figure 7.2) further restricts water exit from the valley, resulting in riverine flooding. Surrounding hills - notably Shivapuri (north), Nagarjun (northwest), Chandragiri (southwest), and Phulchowki (southeast) - act as watersheds, funnelling heavy rainfall into the valley's rivers. The steep slopes and fast runoff increase river levels rapidly, worsening the flooding.

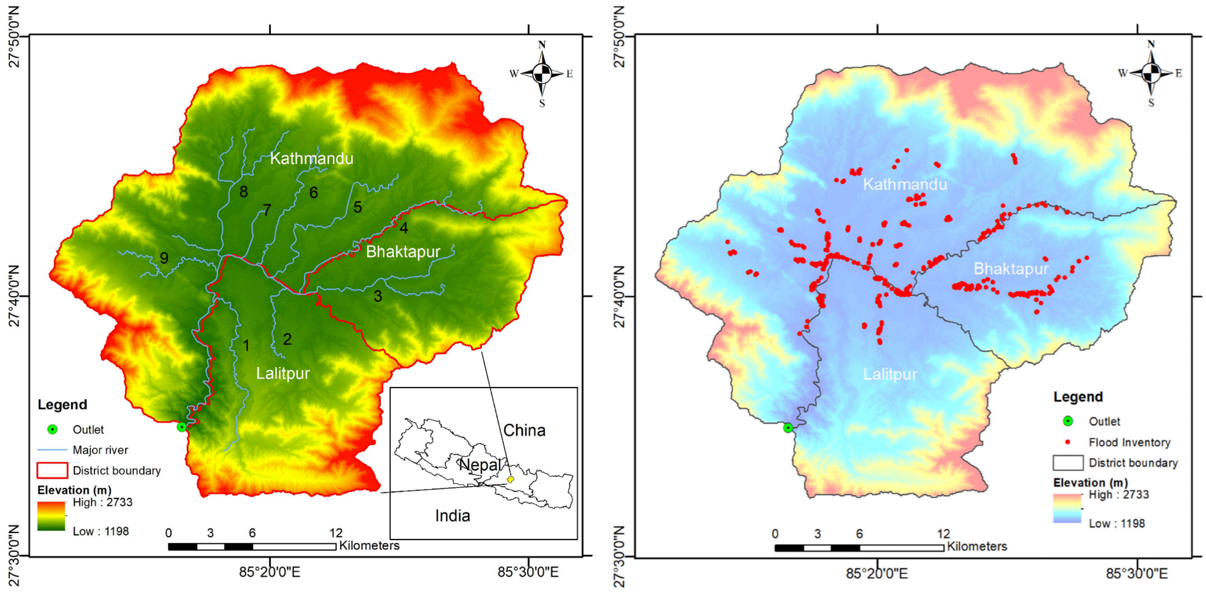

Figure 7.2. *To the left, a map of the Kathmandu Valley's elevation and watershed (rivers: 1—Nakhu Khola, 2—Karmnasha, 3—Hanumante, 4—Manahara, 5—Bagmati, 6—Dhobi Khola, 7—Tukuche, 8—Bishnumati, 9—Balkhu Khola). To the right, a flood inventory map of the Kathmandu Valley, indicating flood events between 1972 and 2022. Source: Chaudhary et al. (2024).*

Chaudhary et al. (2024) suggests that rainfall and elevation are the dominant factors driving flood susceptibility in the valley (see Figure 7.2). Additionally, Chaulagain et al. (2023) stress that distance from the river is significant for flood impact. A 2024 study suggests that flood risk in the Kathmandu valley is increasing, with 2.8 and 12.24% currently facing very high or high flood risk, respectively, while the majority of the valley still faces low (45.30%), moderate (26.80%), or low flood risk (12.80%) (Chaudhary et al., 2024).

Consistent with the areas experiencing the worst impacts in the September 2024 floods, within the Kathmandu Valley, Chaudhary et al. (2024) suggest that the central urban areas are facing the highest flood risk, particularly in Kathmandu Metropolitan City, Lalitpur, and Bhaktapur (see Figure 7.3).

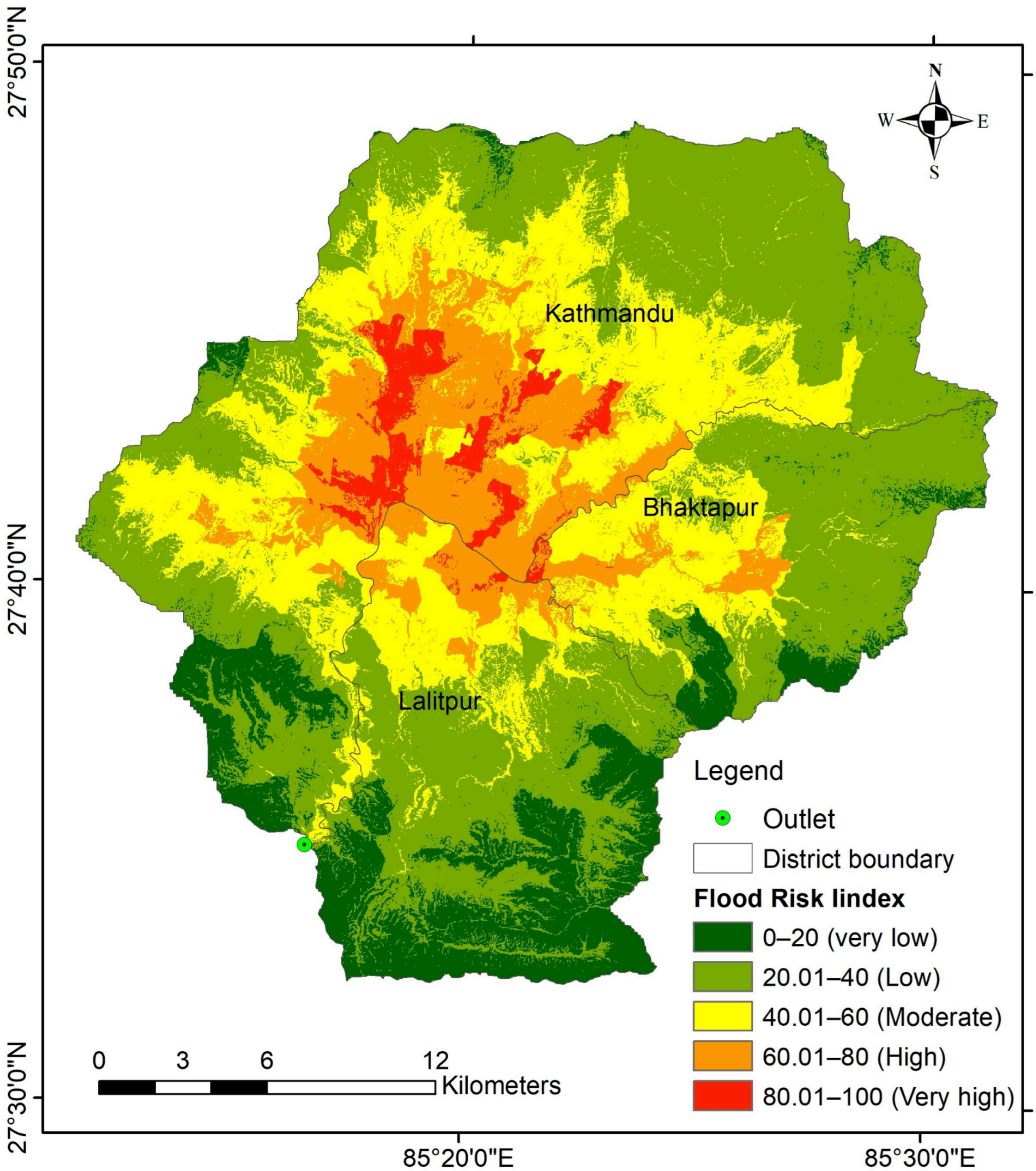

Figure 7.3. *Flood risk index map of Kathmandu Valley. Source: Chaudhary et al. (2024).*

These areas of "very high" flood risk in the Kathmandu Valley are influenced by various factors. Densely populated and largely unplanned urban areas in the southern and central parts of the valley, particularly informal settlements along riverbanks (of, for example, the Bagmati, Bishnumati, and Manohara rivers), face heightened risks due to poor infrastructure and limited access to resources (Chaudhary et al., 2024). Low-income communities are disproportionately affected, as they often reside in flood-prone areas without adequate drainage or flood defences, and have restricted access to education and necessary resources (Dangol, 2024; Mesta et al., 2022). Socio-cultural norms, including traditional views that prioritise men's roles over women's in education and decision-making, further contribute to vulnerability (Goodrich et al., 2019; Udas et al., 2019; Banerjee et al., 2019).

Across all provinces and districts in Nepal, women have lower literacy rates than men (69.4% and 83.6%, respectively) (National Statistics Office, 2021). This gap traps many women in low-income jobs, stalls progress on gender development, and limits their access to vital information on disaster preparedness. Crucially, Chaudhary et al. (2024) identify low literacy, alongside population density, as the key drivers of flood vulnerability in the Kathmandu Valley. Therefore, in Table 7.1, population density and literacy rates are mapped across the worst affected provinces and districts. At province level, Madhesh, one of the eastern provinces of Terai, has the lowest literacy rate among women, at 44.56%, and 36.19% among the average general. Additionally, Madhesh has the highest population density (633 people/km2); over twice that of the second-most densely populated province, Bagmati (301 people/km2), which is home to Kathmandu Valley. At district level, Mahottari, Sarlahi, Siraha, Dhanusha, and Saptari in Madhesh report the lowest literacy rates among women. Despite high literacy rates on average (87,96%), third-highest among the worst-affected districts, Bhaktapur in Bagmati stands out with significant gender disparity, as more than three times as many women as men cannot read nor write (36,250 women and 11,765 men). In the districts of Kathmandu, Lalitpur, Dhankuta, Panchthar, Jhapa, Khotang, Saptari, Udayapur, Solokhumbu, Dolakha, Kavrepalanchok, Ramecchap, and Chitawan, low literacy rates among women is more than double that of men. Not being able to read, in particular, worsens flood risks by limiting people's ability to understand warnings, evacuation orders, and preparedness information, making them more vulnerable during extreme weather events. Further, largely male labour migration from Nepal increases disaster risk by overburdening women with household and agricultural responsibilities, limiting women's capacity to engage in disaster preparedness, and in turn, leaving communities more vulnerable to natural hazards (Upreti & Shrestha, 2017; Jaquet et al., 2016; Hendrickson et al., 2018).

Table 7.1. *Population density and literacy rates across the worst impacted areas in the September floods, based on the Government of Nepal's situational report and the 2021 National Population and Housing Census. Sources: National Statistics Office (2021); Government of Nepal (2024).*

Province	**District**	**Population density (# of people per km2)**	**Literacy rate (% of population above age of 5 years)**		
			Can read and write	**Can read only**	**Cannot read nor write**
Bagmati		301	82,05	0,35	17,57
	Kathmandu	5169	89,22	0,52	10,24
	Bhaktapur	3631	87,96	0,15	11,88
	Lalitpur	1433	88,08	0,17	11,73
	Kavrepalanchowk	261	75,68	0,28	24,02
	Sindhuli	120	72,58	0,23	27,15
	Dolakha	79	72,30	0,42	27,25
	Sindhupalchowk	103	68,04	0,31	31,16
	Ramechhap	110	68,12	0,34	31,52
	Makawanpur	192	77,81	0,25	21,92

	Dhading	169	72,40	0,25	27,33
	Chitawan	325	83,67	0,32	15,99
Madhesh		633	63,53	0,25	25,23
	Dhanusa	735	65,21	0,20	34,55
	Sarlahi	685	60,31	0,19	39,47
	Parsa	485	69,12	0,29	30,56
	Mahottari	706	59,77	0,29	39,91
	Saptari	518	67,69	0,25	32,04
	Siraha	623	53,11	0,29	34,57
Koshi		192	79,68	0,25	20,06
	Dhankuta	169	81,35	0,33	18,29
	Panchthar	139	82,28	0,19	17,51
	Jhapa	621	82,83	0,26	16,89
	Ilam	164	83,37	0,22	16,40
	Morang	619	78,61	0,20	21,17
	Udaypur	165	77,17	0,24	22,57
	Okhaldhunga	130	73,88	0,26	25,84
	Solukhumbu	32	76,94	0,50	22,54
	Khotang	110	75,98	0,31	23,69

7.2 Compounding and cascading events

The September 2024 floods in Nepal were worsened by a series of interconnected factors that compounded and cascaded into a severe disaster.

The 2015 Gorhka earthquake significantly increased flood risk and vulnerability in the Kathmandu Valley through a combination of geophysical and infrastructural impacts. The earthquake destabilised hillsides, triggering widespread landslides, particularly during subsequent monsoon seasons. These landslides heightened the risk of forming landslide dams, which can obstruct rivers temporarily. When these natural dams eventually burst, they release large volumes of water, causing flash floods downstream (Khatakho et al., 2021). This increased risk of landslide-induced floods poses a major hazard to both rural and urban areas of the valley. Most households affected by the earthquake, especially in urban areas, have turned to self-recovery as a common practice, while international and national humanitarian shelter responses have focused their efforts on rural areas, with few agencies active in urban settings (Schofield et al. 2019), putting people in debt traps.

The earthquake caused significant damage to critical infrastructure, including drainage systems, roads, and water supply networks (Gautam & Dong, 2018). The destruction of drainage systems has left many parts of the valley more prone to waterlogging and urban flooding during intense rainfall (Shreevastav et al., 2022). Furthermore, soil liquefaction, which occurred in parts of the valley as a result of the earthquake, has reduced the land's ability to absorb rainwater, thereby increasing surface runoff and flood risk, particularly in areas with dense, unplanned settlements (Mesta et al., 2023). The earthquake's impact on Kathmandu Valley's built environment, including the destruction of both formal and informal housing, compounded the vulnerability of the population to future flooding events. As a result, the valley remains highly susceptible to multi-hazard risks, with flooding now a more prominent threat in the post-earthquake landscape (Khatakho et al., 2021).

Further, with impacts from the COVID-19 pandemic, vulnerability has been exacerbated, particularly for middle and lower-class individuals, who are experiencing greater income losses and increased risk of poverty. Impacts from the pandemic also extends to mental health, for example with increased risk of suicide (Acharya et al, 2020). These factors must be considered in response and recovery planning as they may put further pressure on local communities to recover from a variety of recurring disasters.

As the 2024 monsoon season arrived, these vulnerabilities were further exposed. Intense rainfall overwhelmed rivers like the Koshi, Bagmati, and Narayani, pushing them beyond capacity. The floods were exacerbated by the release of water from both gates of the Kulekhani Dam, only the second such occurrence in 25 years. Road blockages connecting Kathmandu valley with the rest of the country, following several landslides, disrupted essential supply chains, leading to price hikes in basic goods, amplifying economic hardship in the region (The Economic Times, 2024). Furthermore, water released at the Birpur barrage on the Koshi river (18,686 m2/s) and Valmikinagar barrage on the Gandak river (15,914 m2/s) contributed to embankment breaches in Bihar, India (Government of India, 2024). These breaches worsened existing flood conditions (see Figure 7.4), affecting 1.5 million people in areas including Araria, East Champaran, West Champaran, Gopalganj, Supaul, Purnia, and Katihar (Bhelari, 2024; Khan, 2024; Seth, 2024).

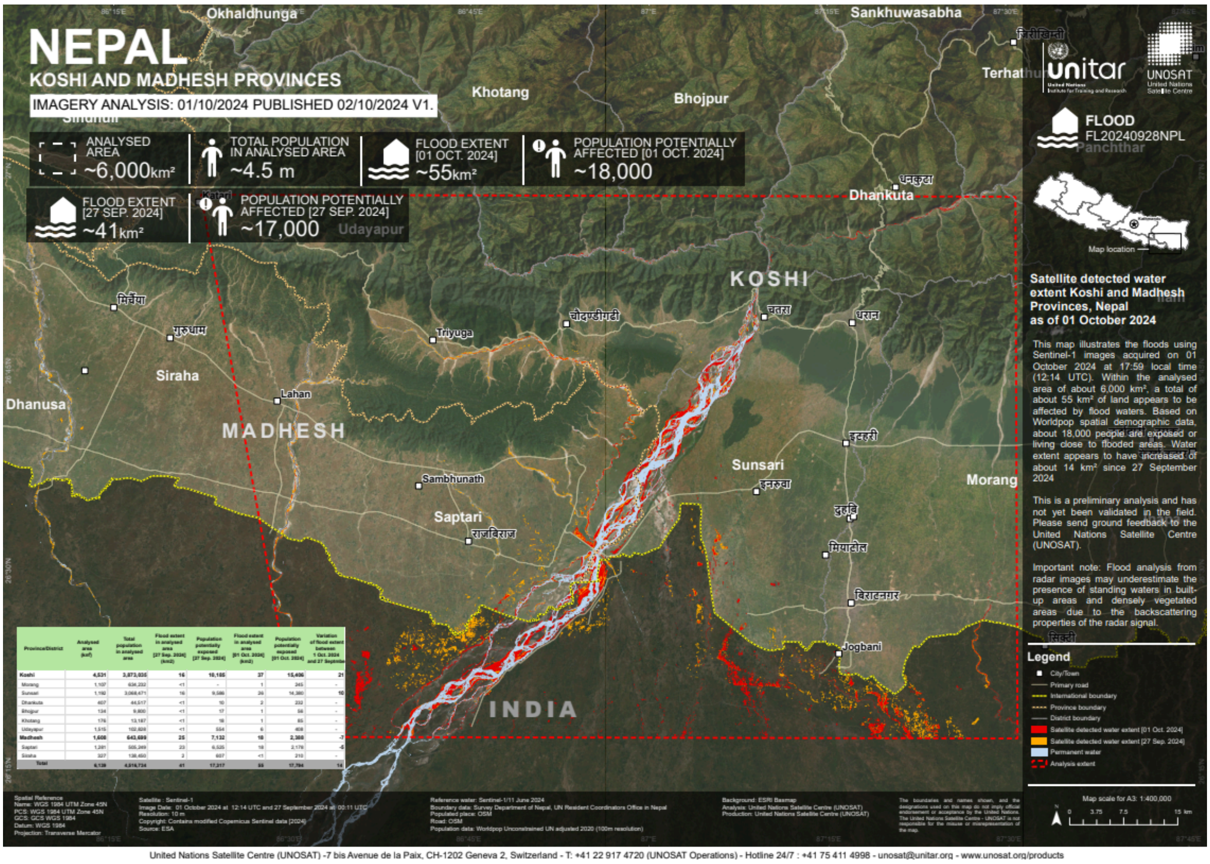

Figure 7.4. *Satellite-detected water extent in Koshi and Madhesh provinces, Nepal, and downstream Bihar province in India, as of 1 October. White illustrates permanent water while orange and red illustrates the water extent on 27 September and 1 October, respectively. Source: UNOSAT (2024).*

7.3 Spatial planning

The Kathmandu Valley, historically a lush and agriculturally productive area (see Figure 7.5), has experienced rapid urbanisation and infrastructure development, leading to significant alterations in land use and heightened flood risk. The valley witnessed a remarkable 386% increase in built-up areas between 1990-2020, the largest among Nepal's major cities (Devkota et al., 2023). This expansion, particularly in Kathmandu District, where agricultural land has decreased by nearly half (Devkota et al., 2023), has disrupted natural water processes, increasing surface runoff and decreasing lateral flow and groundwater discharge (Acharya et al., 2023). Such rapid and unregulated urbanisation has profoundly impacted the region's hydrological dynamics, leading to higher likelihood of flooding.

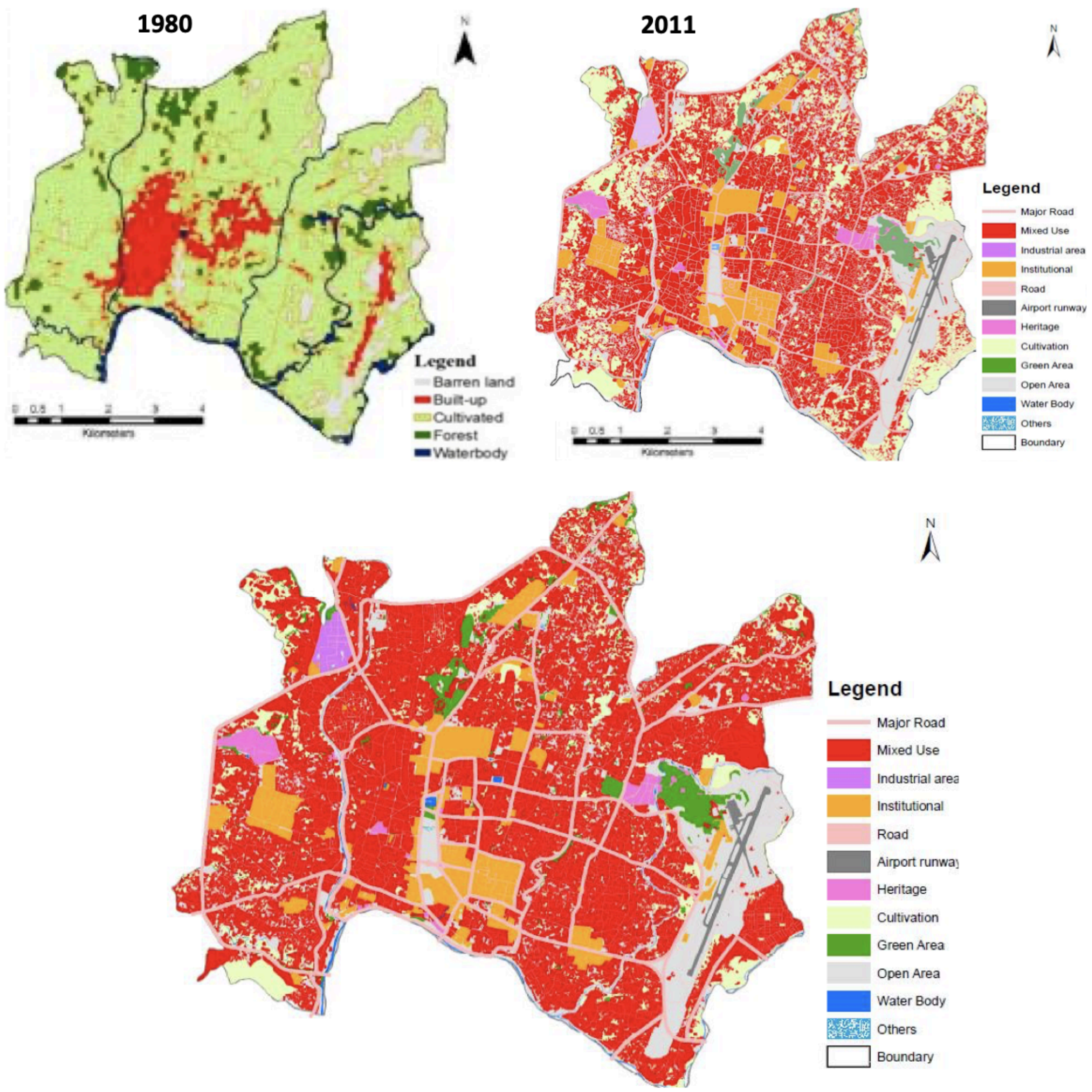

Figure 3. Land use change in KMC: 1980-2019.
Source: Pradhan-Salike and Pokhrel (2017); KMC (2011) and Google Earth Image, 2019.).

Figure 7.5. *Land-use changes in Kathmandu Metropolitan City between 1980 and 2019. Source: Timalsina (2020).*

A study using the SWAT model demonstrated that even a modest 6% increase in built-up areas in the Kathmandu Valley resulted in a 27% rise in average annual discharge (Lamichhane et al., 2024), emphasising the direct link between urban expansion and flood risk. Similarly, a study on flood risk in Sarlahi - one of the hardest-hit districts in the September floods - revealed that land use and land cover changes contributed the most to flooding (40.8%), with built-up areas constituting the biggest risk driver (Shreevastav et al., 2022). Furthermore, reported unauthorised sand mining along rivers destabilises riverbanks, exacerbating the risk of floods and damage, as seen in the recent Roshi River flood in Kavrepalanchowk (Kathmandu Post, 2024) and observed elsewhere in the country, including the Seti Khola river in Pokhara (Fischer et al., 2022). Deforestation, another critical issue, has resulted in the loss of 28% of forest cover between 1989-2019, contributing to soil erosion and sedimentation, which further reduces river capacity and increases flood risks (Shrestha et al., 2022). Unregulated, and sometimes unauthorised, housing development projects adjacent to river and slope land by private sectors (ekantipur.com, 2021, ekantipur.com, 2022) have also resulted in fragile terrain.

Spatial planning efforts in Nepal have aimed to address these challenges, with land-use policies becoming a central focus. The government's eighth five-year plan (1992/93 – 1996/97) identified land use as a key strategy for long-term land management. Subsequent policies, such as the Land Use Policy 2013 and 2015, aimed to regulate urban expansion and conserve natural resources by classifying land into different zones (MoLRM, 2015). The Land Use Act 2019 and the Land Use Regulation (LUR) 2022 further provided a legal framework for categorising land uses and discouraging land fragmentation in urban areas, including the Kathmandu Valley. However, despite these regulations, enforcement has been weak as LUR was amended in 2023 (The Himalayan Times, 2023), and urban sprawl continues unchecked due to limited awareness and supervision by authorities (Chand, 2019, Chitrakar, 2023, Poudel et al., 2023).

Open spaces, crucial for disaster risk management and public life, have drastically diminished in the Kathmandu Valley due to unplanned development (Timalsina, 2020). Historical imagery reveals that as urban areas expand, public open spaces are being lost, making the city more vulnerable in emergencies and negatively impacting social well-being (Timalsina, 2020). Urban flood risks are also exacerbated by inadequate drainage systems, which often fail to cope with intense rainfall, leading to flooding in densely built-up areas like Kathmandu and Banepa.

While there have been efforts to manage flood risks, including constructing embankments and flood barriers along the Bagmati River and other adjoining rivulets in Kathmandu Valley (such as Bishnumati, Dhobi, Nakkhu, Tukucha, Manahara, Hanumante), the implementation has been slow (Dangol, 2024). Further, there tends to be a perception of safety with heavy dependence on these embankments (Raju et al, 2024; Dangol, 2024). As a result, flood risk remains a serious concern. Over-extraction of groundwater, driven by the need for drinking water, construction, and industrial use, has further destabilised the valley's natural water table. It is propelled by a 20% loss in the water distribution system (KUKL, 2023), rapid urbanisation and population growth, an increase in economic activities in the valley, and lifestyle changes (people taking longer showers and washing more clothes) (Augustin, 2022; Ghale, 2023; Ayadi et al., 2020). The over-extraction of groundwater has reduced the soil's ability to absorb rainfall, which could exacerbate flood risks in the future as the ground becomes more compacted (Parajuli & Silwal, 2024).

The expansion of urban areas has also led to the loss of green spaces, formerly forested or agricultural land, and the diversion of natural streams and drainage channels. Many streams have been converted into stormwater drains or covered entirely, limiting their capacity to manage heavy rainfall (Chaulagain et al., 2023). Deforestation in the surrounding hills exacerbates this issue, with eroded soil increasing river sedimentation and reducing the rivers' capacity to handle floodwaters. In some cases, landslides triggered by deforestation and heavy rains have blocked river channels, creating temporary dams that, when they burst, release large amounts of water, causing flash floods (Ibid).

Informal settlements in floodplains, particularly along the Bagmati River, face heightened flood risks due to poor housing conditions and inadequate access to basic services (Arise, 2024). People living in these informal settlements report constant fear of flooding. People have already reported huge financial losses due to loss of infrastructure and housing in the past. Further, narrow alleys and ways provide less mobility for groups with special needs. Residents report living in these hazardous conditions due to lack of choice and heightened vulnerability over the years (ibid.). The flooding potentially has damaging impacts on health and wellbeing in these settings as research has reported poor living conditions and already poor health. More than half of the 40 informal settlements in Kathmandu are located on riverbanks, further exposing them to frequent flood damage (Dangol, 2024). The lack of legal recognition of these settlements exacerbates their vulnerability, as they are often excluded from, or have to contend with inadequate, flood protection measures such as one-sided river embankments (Dangol & Carrasco, 2019; Arise, 2024). Socially marginalised groups, due to the caste system, are at a heightened risk of facing potentially worse impacts as documented in the aftermath of the Nepal earthquake and other cases in the region (Arora, 2022; Otto and Raju, 2023).

7.4 Early warning early action

The Department of Hydrology and Meteorology (DHM) issued special bulletins on 23rd of September and updated on 25th September forecasting heavy to very heavy precipitation and likelihood of flooding & landslides from 26th to 29th September in most districts of the country alerting the civilians and requesting the stakeholder for preparedness. The information was disseminated through social media, radio and television networks, as well as warning messages were sent through SMS alert and ring back tones (see table 7.2). Among the hydrological gauging stations installed in various rivers across the country, 23 stations recorded water levels surpassing the danger level, and an additional 14 stations recorded water levels exceeding the warning level (DHM, 2024). The water flow in the Saptakoshi River has reached the highest level in 56 years. After 22 years, Kathmandu witnessed record rainfall on 27th and 28th. DHM reported that the rainfall on Saturday was the highest ever in the valley's recorded history, surpassing the previous record set in 2002. Rainfall at the Tribhuvan International Airport station in Kathmandu reached 239.7 millimetres in 24 hours, compared to the previous record of 177 millimetres in 2002 (NDRRMA). While a general EWS exists for the Kathmandu Valley, the national EWS is not linked to a community EWS in which the national messages are refined and targeted to the specific communities that may be impacted, as is prevalent in other parts of Nepal (e.g. Bardiya and Kaliali districts).

Table 7.2. *Information dissemination between 26-29 September. Source: DHM (8 October, 2024).*

Information	**Meteorological Forecasting Division**	**Flood Forecasting Division**
Monsoon special Bulletin	2	1
Regular Bulletin	8	4
# of phone calls recieved	~1,105	~1,049
Facebook posts	17	58
Twitter posts	17	51
# of email recipients	~304	~1,032
# of SMS Alert (event number)	-	49
SMS	-	4,093,795
Live program	~11 (TV), ~14 (FM)	5 (TV), 10 (FM)

Phone calls from security agencies	3	7
Phone calls from media	~43	33
Command Post Meetings at NEOC (Briefing by DDG and DG on 23 and 28 September)	2	

The Nepal Red Cross Society activated its Simplified Early Action Protocol (EAP) for the Karnali Province and the Far West in September 2024, in response to forecasted heavy rainfall and flooding (Anticipation Hub, 2024). However, the activation was halted after actual precipitation and flood levels were significantly lower than predicted in the western part of Lumbini, Karnali, and Sudurpaschim provinces, whereas higher than expected in eastern and central Nepal. The flooding was forecasted as medium to very high risk for 10 rivers in the country. However, these systems do not cover the Kathmandu Valley, which was most impacted by the 2024 floods.

While a series of flood warning messages were issued, it remains to be understood whether they reached or were understood by the people in the path of the extreme rainfall. In the DHM's forecasts, a large area of the country was designated in the "red zone" (half the country), likely making it difficult for decision makers to determine which areas were at highest risk of impacts and where to initiate early actions. Some people do not have access to early warning messages because they do not have access to a phone or internet, or may not understand the potential implications of being in the "red zone." In particular, the current forecasts and warnings could be improved to take into account the existing exposure and vulnerability level of the forecasted area, and further target those communities at highest risk of impacts with appropriate early actions.

7.5 Emergency preparedness and response

In response to the devastating flooding, the government deployed 30,731 security personnel across the affected districts, rescuing more than 17000 people, out of which 910 were heli-rescued (NDRRMA, 2024). Thousands of others were rescued by humanitarian organisations like the Nepal Red Cross Society, civilians, and communities. The initial Rapid Assessment (IRA) has been carried out in support of the Red Cross in most of the affected areas and NPR 4.32 million (~ UDS 32,481) has been distributed as cash assistance to families of deceased individuals, injured and for house damaged in the affected districts. Food support and non food items have been distributed to 2,757 affected families by humanitarian organisations and national/international development organisations. Further, the National Disaster Management Executive Committee under the Ministry of Home Affairs has announced compensation of around NPR 200,000 (~ USD 1,485) to families of individuals who have lost their lives due to the floods and landslides or are missing for over 10 days, and NPR 50,000 (~ USD 371) in two instalments for construction of temporary shelter (Mathrubhumi, 2024).

Despite reports of extensive relief and response efforts from national authorities and humanitarian organisations, some victims have voiced concerns that aid has not reached them (Poudel, 2024). The National Human Rights Commission (NHRC) has criticised the government's relief initiatives, indicating that distribution has been less than satisfactory, even in regions near the capital.

Despite the efforts, several of the affected communities are disconnected from the road network, power outage, communication networks like telephone and mobile, devoid of the water and sanitation facilities, placing them at greater health and safety risks. In the midst of these challenges, private sector efforts have emerged to provide assistance to those in need. Notably, the Bhatbhateni, Nepal's largest supermarket chain, has donated NPR 1 crore 11 lakh (~ USD 83,459), alongside food worth NPR 80 lakh (~USD 142,000) for the affected (Deshsanchar, 2024a). Similarly, the Non-Resident Nepali Association (NRNA) has pledged NPR 1 crore (~USD 75,000) for relief and rescue (Deshsanchar, 2024b). Other organisations such as the Federation of Nepal Chamber of Commerce (~USD 742) and Industry and Citizens Bank (~ USD 18,500) have also made substantial contributions to the Prime Minister's Disaster Relief Fund.

Owing to the magnitude of devastation and the anticipated response needs ahead, Nepal has sought assistance from the international community. Minister Nawal Kishor Sah Sudi, Chairman of the Social Welfare Council, has made an urgent appeal to international NGOs for support in addressing the crisis (The Rising Nepal, 2024). Some swift responses to this appeal have been made. So far these include a donation of USD 100,000 to the Nepal Red Cross Society from the Red Cross Society of China (Pati, 2024). Further, the British Embassy in Nepal has pledged £400,000 through Start Fund Nepal to meet immediate needs such as food, health services, and protection for the most affected (UN Resident Coordinator in Nepal, 2024). Likewise, IFRC has launched the Disaster Response Emergency Fund (DREF) of 520,718 CHF to immediately respond to this situation addressing the needs of immediate shelter, water, sanitation and hygiene, health services with the focus on mental health. To address the immediate needs of the affected population, multi purpose cash assistance has also been planned. The DREF operation has targeted the Bagmati and Gandaki province (IFRC, 2024).

V&E conclusions

Historically, the Kathmandu Valley region is not the focus of flood risk management efforts in Nepal, as other regions (notably Terai) generally have been classified as high risk and have historically seen highly impactful floods. For example, a considerable number of anticipatory action initiatives for floods focus on the western and eastern part of the country, but not on Kathmandu Valley. This event underscores that even regions that may be at a relatively lower risk than other parts of the country can see large flood impacts, and require flood risk management efforts especially as the urban landscape changes over time.

Rapid urbanisation (386% increase in built up areas between 1990-2020) and deforestation (28% reduction in forest cover over 1989-2019) in the Kathmandu Valley has disrupted natural water processes, increasing surface runoff and overwhelming drainage systems, while building on flood plains and near rivers has increased the exposure of people and assets to these events. The 2015 Gorhka earthquake further destabilised hillsides and weakened drainage infrastructure, compounding the vulnerability to floods and landslides. Low-income communities and informal settlements along riverbanks are disproportionately affected by floods due to poor infrastructure, inadequate access to resources, and limited disaster preparedness. These populations face heightened risk, with low literacy rates, particularly among women, further restricting their access to disaster information and resources.

While policies and regulations exist, challenges with implementation and enforcement have left the valley vulnerable to the increasing impacts of floods. Comprehensive spatial planning, combined with disaster risk reduction and adaptation, effective policy enforcement, and increased public awareness, are crucial to mitigate flood risks across central and eastern Nepal, including Kathmandu Valley.

Data availability

All time series used in the attribution analysis are available via the Climate Explorer.

References

All references are given as hyperlinks in the text.